Preflight and In-Flight Calibration Plan for ASTER

A. ONO AND F. SAKUMA

National Research Laboratory of Metrology, Tsukuba, Japan

K. ARAI

Saga University, Saga, Japan

Y. YAMAGUCHI

Geological Survey of Japan, Tsukuba, Japan

H. FUJISADA

Electro-technical Laboratory, Tsukuba, Japan

P. N. SLATER AND K. J. THOME

Optical Sciences Center, The University of Arizona, Tucson, Arizona

F. D. PALLUCONI

Jet Propulsion Laboratory, Pasadena, California

H. H. KIEFFER

U.S. Geological Survey, Flagstaff, Arizona

(Manuscript received 17 March 1995, in final form 1 August 1995)

ABSTRACT

Preflight and in-flight radiometric calibration plans are described for the Advanced Spaceborne Thermal Emission and Reflection Radiometer (ASTER) that is a multispectral optical imager of high spatial resolution. It is designed for the remote sensing from orbit of land surfaces and clouds, and is expected to be launched in 1998 on NASA's EOS *AM-1* spacecraft. ASTER acquires images in three separate spectral regions, the visible and near-infrared (VNIR), the shortwave infrared (SWIR), and the thermal infrared (TIR) with three imaging radiometer subsystems. The absolute radiometric accuracy is required to be better than 4% for VNIR and SWIR radiance measurements and 1 to 3 K, depending on the temperature regions from 200 to 370 K, for TIR temperature measurements.

A reference beam is introduced at the entrance pupil of each imaging radiometer to provide the in-flight calibration. Thus, the ASTER instrument includes internal onboard calibration units that comprise incandescent lamps for the VNIR and SWIR and a blackbody radiator for the TIR as reference sources. The calibration reliability of the VNIR and SWIR is enhanced by a dual system of onboard calibration units as well as by high-stability halogen lamps. A ground calibration system of spectral radiances traceable to fixed-point blackbodies is used for the preflight VNIR and SWIR calibration.

Because of the possibility of nonuniform contamination effects on the partial-aperture onboard calibration, it is desirable to check their results with respect to other methods. Reflectance- and radiance-based vicarious methods have been developed for this purpose. These, and methods involving in-flight cross-calibration with other sensors are also described.

1. Introduction

ASTER (Advanced Spaceborne Thermal Emission and Reflection Radiometer) is a multispectral optical imager of high spatial resolution for earth remote sensing from orbit (Fujisada and Ono 1991; Fujisada 1994). The instrument is provided by the Japanese Ministry of International Trade and Industry (MITI) to

Corresponding author address: Dr. F. Sakuma, Thermophysical Metrology Dept., National Research Lab of Metrology, 1-1-4 Umezono, Tsukuba-Shi, Ibaraki 305, Japan.

be flown on the National Aeronautic and Space Administration's (NASA) Earth Observing System (EOS) *AM-1* spacecraft that is scheduled to be launched into a polar orbit in 1998.

a. Science goals

The major features of ASTER measurements are high-spatial-resolution imaging of land surfaces, inland waters, ice and clouds with a total of 14 bands from the visible to the thermal infrared, and in-track stereoscopic viewing for land surface and cloud topography. ASTER data will be used for research of solid earth process, climate and hydrology process, biogeochemical dynamics, earth system history, and human interaction. Synergistic effects will be explored by combining ASTER data with those from the other instruments on the EOS *AM-1* spacecraft, that is, MODIS, MISR, CERES, and MOPITT, which are described elsewhere in this issue.

ASTER development is presently in the proto-flight model (PFM) phase where instrument calibration is one of the central issues. Remote sensing user's requirements for instrument calibration were identified in the design phase to assure instrument data quality. Then an instrument calibration plan was established to meet the calibration requirements.

b. Instrument description and radiometric performance

The observation performance of the ASTER instrument is specified in Table 1. There are a total of 14 spectral bands in the visible and near-infrared (VNIR), the shortwave infrared (SWIR), and the thermal infrared (TIR) for nadir observation. The center wavelengths and bandwidths in the VNIR were selected to be the same as those of OPS (optical sensor on *JERS-1*) for data continuity. While band 3N is nadir looking, band 3B is backward looking to take stereoscopic images in the along-track direction with the same spectral and spatial characteristics as band 3N. The base-to-height ratio of stereoscopic viewing is chosen to be 0.6 between bands 3B and 3N, which is a significant improvement over the 0.3 of OPS.

The number of bands in the SWIR is increased from 4 for OPS to 6 for ASTER, and the bandwidth is decreased significantly to enhance the discrimination of mineral species. Five TIR bands are added for temperature and emissivity measurements.

Specified ground spatial resolutions are 15 m for the VNIR, 30 m for the SWIR, and 90 m for the TIR at the 705-km spacecraft altitude in a circular orbit. Radiometric resolutions of individual bands are specified in Table 1. The output signal quantizations are 8 bits for VNIR and SWIR, and 12 bits for the TIR. The swath width is 60 km on the ground from edge to edge (4.9° field of view) for all bands in the nadir direction with cross-track pointing capability of ±116 km (±8.55°) off nadir. Only the VNIR has cross-track pointing capability specifically enhanced up to ±314 km (±24°) off nadir.

TABLE 1. Requirement concerning center wavelength, bandwidth and S/N or NEΔT of ASTER bands.

Radiometer	Band number	Center wavelength (μm)	Bandwidth (μm)	S/N or NEΔT
VNIR	1	0.56	0.08	≥140
	2	0.66	0.06	≥140
	3N	0.81	0.10	≥140
	3B	0.81	0.10	≥140
SWIR	4	1.650	0.10	≥140
	5	2.165	0.04	≥54
	6	2.205	0.04	≥54
	7	2.260	0.05	≥54
	8	2.330	0.07	≥70
	9	2.395	0.07	≥54
TIR	10	8.30	0.35	≤0.3 K
	11	8.65	0.35	≤0.3 K
	12	9.10	0.35	≤0.3 K
	13	10.60	0.70	≤0.3 K
	14	11.30	0.70	≤0.3 K

The VNIR optics are basically a mirror system of 80-mm aperture diameter for both nadir and backward looking, with compensation lenses for high optical performance (Takahashi et al. 1991). Cross-track coverage is provided by a 5000-element linear array CCD of silicon photodiodes. Three linear CCDs are located on the focal plane physically separated but simultaneously sampling the same area perpendicular to the along-track direction for the nadir-looking radiometer, while a single linear CCD is used for the backward-looking radiometer. Spectral separation is made with beam splitters, and the spectral bands are located with interference filters just in front of the CCD detectors. The cross-track pointing is obtained by rotating both VNIR telescopes together with a stepping motor.

The SWIR optics are a lens system of 190-mm aperture diameter (Akasaka et al. 1991). The cross-track coverage is provided by a 2048-element linear array CCD detector of platinum silicide Schottkey barrier photodiodes. Twelve linear CCDs (six pairs of staggered arrays) are located on a single chip perpendicular to the along-track direction. They do not sample the same area simultaneously. The spectral bands are defined by interference filters just in front of the individual CCD detectors. The cross-track pointing is obtained by rotating a flat mirror in front of the telescope.

The TIR optics consist of a Newtonian mirror system with a 280-mm aperture diameter (Aoki et al. 1991). Whiskbroom scanning takes place in the cross-track direction by vibrating a flat mirror, which is mechanically nonresonant and electrically driven, in front of the telescope. The focal plane is composed of small-scale (10 element) linear array detectors for each band (a total of

50 elements) of mercury–cadmium–telluride photoconductive detectors, which are located parallel to the along-track direction. The spectral bands are defined by interference filters just in front of the individual detectors. A mechanical chopper is inserted at the primary focal plane during the reverse scan of the scanning mirror to provide ac output signals. The temperature of the mechanical chopper is monitored as well as that of the optical barrel, mirrors, relay lenses, etc. to compensate for the temperature drift of the offset. The cross-track pointing is obtained by rotating the whole cross-track scanning unit.

TABLE 2. Knowledge requirement on absolute responsivity and offset, and control requirement on the rejection of stray light.

Radiometer	Absolute accuracy	Offset at the normal gain	Stray-light rejection
VNIR	≤ ±4%	≤ ±1 DN	≤1%
SWIR	≤ ±4%	≤ ±1 DN	≤1%
TIR			
200–240 K	≤ ±3 K		
240–270 K	≤ ±2 K	n/a	≤1%
270–340 K	≤ ±1 K		
340–370 K	≤ ±2 K		

c. Calibration requirements

Calibration accuracies of absolute responsivity for the VNIR and SWIR are required to be better than ±4% at a confidence level of 68% (±1 sigma). The requirement is specified at individually defined, high-level input radiances in the VNIR and SWIR bands. The accuracy of radiance measurements is assured by the knowledge requirements of absolute responsivity and offset, and a control requirement of stray light rejection as listed in Table 2, as well as by a knowledge requirement of nonlinearity of response, which is specified separately to be less than ±1% for the VNIR, SWIR, and TIR (A. Ono 1994, unpublished manuscript). Calibration accuracies of the TIR temperature scale, which depend on temperature regions, are listed in Table 2. These are required with a one-sigma confidence level. These specifications are to be met until the end of expected instrument life, that is, 5 years in orbit.

The knowledge requirements for the offsets of the individual bands in the VNIR and SWIR are selected to ensure accurate radiance measurement in orbit at low light levels as well as at the defined high level. The specification is intended to validate radiance measurement accuracy at low levels as well as at the defined high level. The stray-light rejection is defined as the relative response difference of the radiometer between viewing a standard source in the preflight calibration phase and viewing a source of the same radiance level whose angular extent is equivalent to the whole earth disk as seen from orbit. This specification is intended to validate radiance measurement accuracy for the size-of-source effect of the radiometer.

d. Calibration concepts

ASTER radiometric calibration is divided into two phases, preflight and in-flight. In the preflight phase, the instrument, including imaging radiometers and the internal onboard calibration units described later in this section, is calibrated against standard sources (Ono and Sakuma 1991). The requirements for the standard sources are a large aperture diameter to fill the radiometer apertures (80 mm for VNIR, 190 mm for SWIR, and 280 mm for TIR), homogeneous radiance over the source aperture, and accurately calibrated spectral radiances. It should be noted that the preflight calibration uncertainty must be considerably smaller than the specified total uncertainty because it excludes in-flight calibration uncertainty. Thus the required accuracy levels of ASTER preflight calibration are comparable with or rather higher than those of spectral radiometers for ground use.

In the in-flight phase, the instrument will be operated in orbit for 5 years without any human access. It is reasonable to assume that the instrument performance will change in orbit due to contamination and degradation of optical components, detectors, electronics, etc. This necessitates appropriate preparation of internal onboard calibration units to be used for periodic calibrations of the radiometer in orbit.

An onboard calibration unit introduces a well-defined reference beam to the radiometer at the front end to calibrate the whole radiometer system. Since an onboard calibration unit is also a kind of optical–radiative system, its performance can change in orbit due to contamination and degradation. Thus, the onboard calibration unit has to be designed to be more reliable than the ASTER radiometer itself. A two-point calibration is the basic approach in the reflected solar region (VNIR and SWIR) to determine the offset and the responsivity. A high-level input is given by an onboard calibration unit, while a zero-level input is given by the night side of the earth. The onboard calibration unit consists of a highly stable halogen lamp as a radiation source, optics to collect radiation from the lamp and direct it as a reference beam to the radiometer, and photodetectors to monitor the lamp radiance and/or the reference beam flux.

High-stability halogen lamps are used, based on the experiences of OPS calibration. To minimize the possibility of the onboard calibration unit becoming contaminated and degraded in orbit, the onboard calibration unit design is as simple as possible. Also dual onboard calibration systems are used to enhance reliability. The two identical onboard calibration units cross-check the performance of each other periodically in orbit. If any change is detected between consecutive in-flight calibrations, it is possible to infer and identify which component has changed: the ASTER radiometer, the halogen lamp, the calibration optics, or the photo-

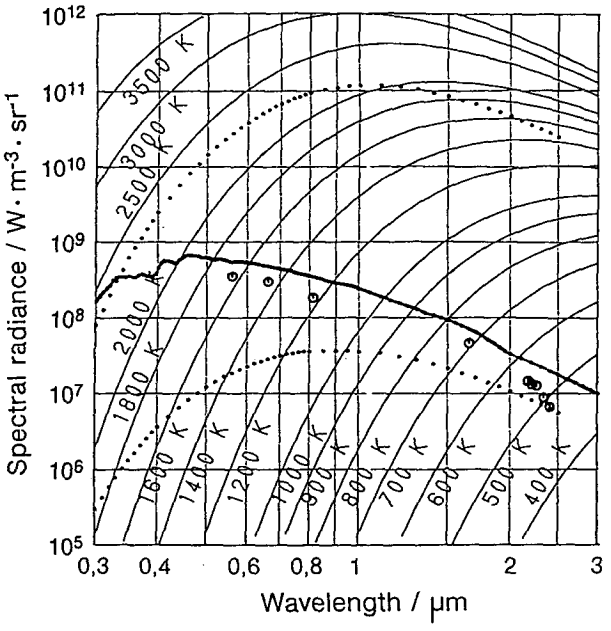

FIG. 1. Spectral radiance of blackbodies (thin solid lines), spectral radiance standard lamp (upper dotted line), reflected solar radiation (thick solid line), spectral irradiance standard lamp (lower dotted line), and high-level input radiances of VNIR and SWIR bands (circles).

detector. The radiometer's radiance data are corrected for the identified change.

For the thermal emission region (TIR), two-point calibration is also desirable, for example, an onboard blackbody radiator at the environmental temperature for a high-level input and cold space for a low-level input. However, the present ASTER instrument design does not allow the TIR radiometer to view cold space due to mechanical and spacecraft interface reasons. Thus it was decided to vary the temperature of the onboard blackbody radiator over about 70 K. The TIR temperature scale is interpolated within and extrapolated outside the variable temperature range.

The temperature of the onboard blackbody radiator is measured accurately. The emissivity and radiative environments are well characterized to evaluate the emissive component as well as the reflective component. Emissivity change is also estimated due to contamination and degradation in orbit. Since the onboard calibration unit for the TIR is just a blackbody radiator and thermometers, a single system is acceptable instead of a dual one. But multiple thermometers are used to cross-check each other.

2. Preflight calibration/characterization methodology

a. Radiometric calibration

1) REFLECTANCE BANDS—PREFLIGHT CALIBRATION APPROACH

Figure 1 shows spectral radiance levels of reflected solar radiation and standard sources. It is seen from this figure that the spectral radiance standard lamp provides higher levels than that of the reflected solar radiation by 2–4 orders of magnitude depending on the spectral region. The spectral irradiance standard lamp provides comparable levels with the reflected solar radiation in the SWIR region while providing levels lower than that by an order of magnitude in the VNIR spectral region. On the other hand, blackbody radiation closely approximates the high-level input radiances required for calibration, if the blackbody temperatures are selected appropriately.

The levels of the spectral radiance standard lamp are too high to be used as a standard source for the VNIR and SWIR calibrations. The levels of the spectral irradiance standard lamp seem to be acceptable for the VNIR and SWIR calibration. However, the spectral irradiance standards have not yet been established very accurately, and a well-maintained, accurately characterized, white diffuser is necessary.

Considering that fixed-point blackbodies have become commercially available at several temperature levels, it is reasonable to take fixed-point blackbodies as standard sources whose temperatures are precisely given by the International Temperature Scale of 1990 (ITS-90). The available temperature range is from 231.928°C (tin point) up to 1084.62°C (copper point). As seen in Fig. 1, blackbody radiation spectra have a steep slope where the spectral radiance increases with increasing wavelength in the spectral regions of interest. So high-wavelength accuracy is needed when making spectral radiance calibrations against blackbody radiation.

The system designed for ASTER VNIR and SWIR preflight calibration consists of standard sources and measuring apparatuses of spectral radiances. Fixed-point blackbodies will be used as primary standards, variable temperature blackbody furnaces will be used as transfer standards, and internally irradiated integrating spheres as working standards. Spectral radiance meters are to be used for the calibration of transfer and working standard sources. The preflight calibration system for the VNIR and SWIR will basically follow that for the OPS preflight calibration.

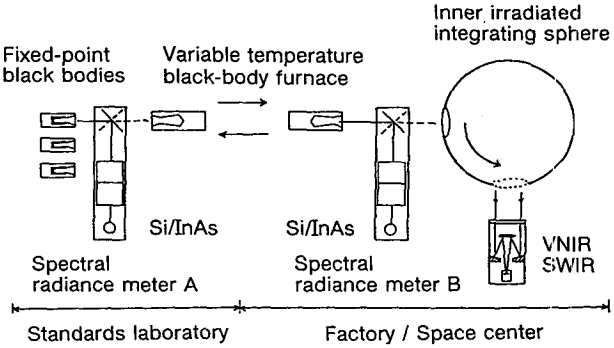

FIG. 2. Preflight calibration system for VNIR and SWIR.

TABLE 3. Estimate of the uncertainties of the preflight and in-flight calibration of the ASTER VNIR and SWIR.

	Error factor	VNIR	SWIR
Preflight calibration	Fixed-point blackbody	±0.3%	±0.6%
	Radiance meter A	±0.6%	±0.7%
	Transfer standard blackbody	±1.5%	±0.9%
	Radiance meter B	±0.8%	±1.5%
	Integrating sphere	±0.7%	±2.0%
	Radiometer	±0.3%	±0.3%
	Onboard halogen lamp	±0.5%	±0.5%
	Lamp monitor	±0.5%	±0.5%
	Air-vacuum shift	±0.7%	±0.7%
	Subtotal	±2.2%	±3.0%
In-flight calibration	Thermal change of lamp monitor	±0.3%	±0.3%
	Long-term stability of lamp monitor	±1.0%	±1.0%
	Lamp monitor measurement error	±0.3%	±0.3%
	Lamp positioning	±0.3%	±0.3%
	Gravity shift	±2.0%	±2.0%
	Radiometer measurement error	±0.3%	±0.5%
	Difference in full/partial aperture	±2.0%	±0.5%
	Subtotal	±3.1%	±2.4%
Total		±3.8%	±3.8%

Figure 2 shows schematically the preflight system that was used for OPS calibration (Sakuma and Ono 1991). Commercially available fixed-point blackbody furnaces of tin, lead (327.46°C), zinc (419.527°C), silver (961.78°C), and copper were used as primary standards with a temperature accuracy of 0.1°C and a plateau duration of about 10 min (Sakuma and Hattori 1982). Two types of variable-temperature blackbody furnaces were used as transfer standards: a blackbody cavity made of copper whose temperature is controlled and measured by a platinum resistance thermometer in the medium temperature range from 50° to 450°C, and a blackbody cavity made of silicon carbide whose temperature is controlled and measured by a platinum–rhodium thermocouple in the high-temperature range from 800° to 1450°C. The variable temperature blackbody furnaces were calibrated against the fixed-point blackbodies by using a spectral radiance meter that includes a switching mirror to select a target, double-grating monochromator, and photodetectors (a silicon photodiode for the VNIR and an indium–arsenide photodiode for the SWIR). The spectral radiance of the variable temperature blackbody furnaces was measured in the VNIR and SWIR spectral range, and the radiant characteristics were expressed with two parameters, that is, the effective temperature T_e and the cavity emissivity ϵ_c (Hattori and Ono 1982) as defined by Eq. (1):

$$L(\lambda) = \epsilon_c L_b(\lambda, T_e), \quad (1)$$

where $L(\lambda)$ is the spectral radiance of a variable temperature blackbody furnace and $L_b(\lambda, T_e)$ is Planck's equation for blackbody spectral radiance.

The variable temperature blackbody furnaces calibrated at the Japanese National Research Laboratory of Metrology (NRLM) were transported to the OPS contractor's factory to calibrate a large aperture integrating sphere that served as a working standard. The integrating sphere, internally coated with barium sulfate, was of 1-m inner diameter and 280-mm aperture diameter with 12 halogen lamps around the aperture inside the sphere (Suzuki et al. 1991). The lamps were operated at a constant dc voltage. The level of spectral radiance was adjusted by changing the number of operating lamps and the dc voltage.

The ASTER VNIR and SWIR preflight calibration system is to be an improvement over that developed for the OPS. Some problems were experienced with the reproducibility of a high-temperature blackbody furnace when transported from the NRLM to the contractor's factory, so a more reproducible high-temperature blackbody furnace will be made, or the contractor's engineers will be asked to calibrate a high-temperature blackbody furnace against the fixed-point blackbodies using their own spectral radiance meter B at the factory.

In the ASTER VNIR preflight calibration, high-temperature blackbody furnaces have to be calibrated at significantly higher temperatures (1383° and 1172°C) than the copper point (1085°C), so the linearity of response of the spectral radiance meter A will be carefully investigated above the copper point.

Table 3 shows an estimate of the uncertainty of the preflight calibration of the ASTER VNIR and SWIR. The uncertainty of the spectral radiance meter B is mostly due to the wavelength uncertainty. The main factor in the uncertainty of the integrating sphere is the nonuniformity of the spectral radiances at the aperture of the sphere, which is larger in the shortwave infrared region than in the visible or near-infrared regions. The main cause of the air-vacuum shifts is that the lamp bulb is not cooled by convection when operated in a vacuum.

The final radiometric preflight calibration may be carried out in a thermal vacuum chamber. The integrating sphere, located outside, will be viewed through a vacuum window. The total uncertainty of the preflight calibration is estimated to be in the range ±2% to ±3%.

2) THERMAL BANDS

Figure 3 shows schematically the TIR radiometer and an onboard blackbody radiator. In the calibration mode the pointing mirror of the TIR turns around so the radiometer can view the onboard blackbody. The temperature of the onboard blackbody is measured by platinum resistance thermometers. The onboard blackbody is cooled radiatively in orbit and is usually controlled to 270 K by electric heaters for low-temperature calibration. It is occasionally heated to 340 K for high-temperature calibration.

The preflight calibration of the TIR will be carried out in a thermal vacuum chamber against the onground standard blackbody shown in Fig. 4. The standard blackbody whose temperature ranges from 100 to 370 K simulates zero radiance and covers the whole dynamic range of the TIR. The emissivity of a cavity-type standard blackbody should be higher than 0.998 to assure the required accuracy of the TIR in its temperature range. The temperatures of the standard blackbody are measured by platinum resistance thermometers traceable to the NRLM.

In the preflight calibration, the output V of each band of the TIR is correlated with the radiance temperature S of the standard blackbody by the equation

$$V(S) = C\left\{\exp\left[\frac{c_2}{(AS + B)}\right] - 1\right\}^{-1} + D, \quad (2)$$

where c_2 is the second radiation constant and A, B, C, and D are coefficients to be determined in the preflight calibration. A and B are related to the spectral characteristics of the radiometer operating bands, while C and D are related, respectively, to the responsivity and offset of the radiometer.

The spectral radiance (or radiance temperature) of the onboard blackbody system, including reflection components of the environmental radiation, will be determined at selected temperature levels against the standard blackbody and will be correlated to temperatures of the onboard blackbody and the environment.

The offsets of individual radiometer bands will be determined against a near-zero radiance source that is simulated by the standard blackbody cooled to a sufficiently low temperature. The offsets will be correlated with the temperatures of the pointing mirror, primary mirror, secondary mirror, telescope barrel, lens holder, and chopper unit as well as the onboard blackbody.

b. Spectral characterization

The spectral responsivities of the ASTER bands are specified by center wavelengths, bandwidths, band edge responses, flatness of in-band responses, and suppression of out-of-band responses. The band edge response is defined by the wavelength difference between 10% and 80% of the peak responsivity. The flatness of in-band response requirement is such that the responsivity shall be larger than 80% of the peak value in the wavelength region between two wavelengths corresponding to 80% responsivity of the peak at which the band edge response is defined. The suppression of out-of-band responses is such that the integrated contribution from the region below 10% of the peak responsivity shall be less than 3% of the integrated in-band response.

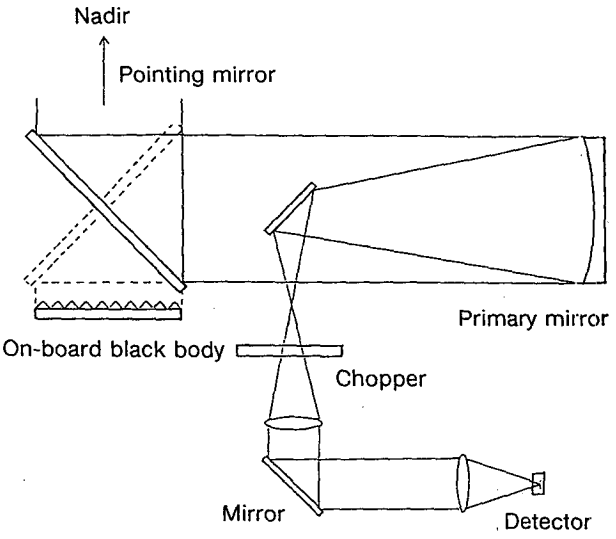

FIG. 3. TIR radiometer subsystem with an onboard blackbody radiator.

The in-band and out-of-band spectral responsivities of the VNIR bands will be measured at the system level for five detector elements of each band by using a collimator system with filters at 5-nm intervals. The five detector elements will be located at the center, both ends, and one quarter in from each end. The spectral characteristics of each optics component, especially the interference filter and the detector will also be measured separately, multiplied together, and compared to the result of the system-level measurement.

The measurement of the spectral characteristics of the SWIR will be similar to the VNIR except that the calibrator will be a collimator system with a grating monochromator. Because the bandwidths of the SWIR bands 5 and 6 are 40 nm, the knowledge of the center wavelengths and bandwidths of these SWIR bands should be better than 2 nm. The spectral responsivities of the TIR bands will be measured separately in each optical component for five detector elements in each band, as described earlier. The spectral characteristics of the detector combined with the filter will be measured by using a Fourier transform interferometeric ra-

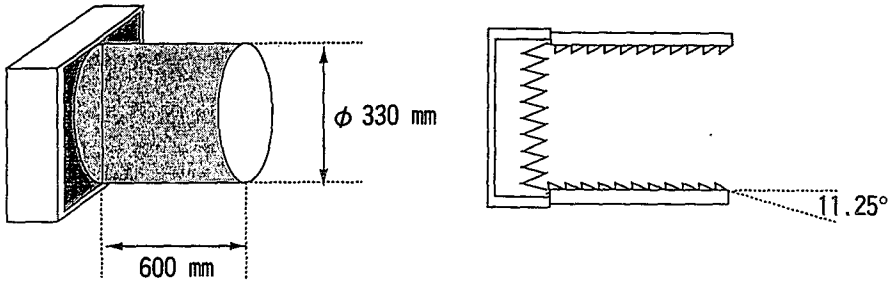

FIG. 4. Onground standard blackbody for TIR calibration.

diometer (FTIR) with a minimum spectral resolution of 0.5 cm^{-1}. The accuracy of wavelength measurement by using the FTIR is about 10 nm.

3. Instrument cross-calibration

a. Preflight cross-calibration

Recently many satellite optical sensors for earth observation have been developed and operated, but no one sensor covers the needs of the user community with respect to lifetime, spatial and spectral resolution, observation frequency, and so on. So the combined use of data from different sensors has been necessary. For this reason, the radiometric and spectral calibration in the preflight phase are very important. Round-robin (RR) radiometers have been developed at NRLM (Sakuma et al. 1994), NIST, and The University of Arizona (Biggar and Slater 1993) for the intercomparison of the working standard spherical integrating sources (SIS) of EOS *AM-1* instruments, especially among ASTER, MODIS, and MISR. The EOS *AM-1* RR experiments have been in operation since 1994.

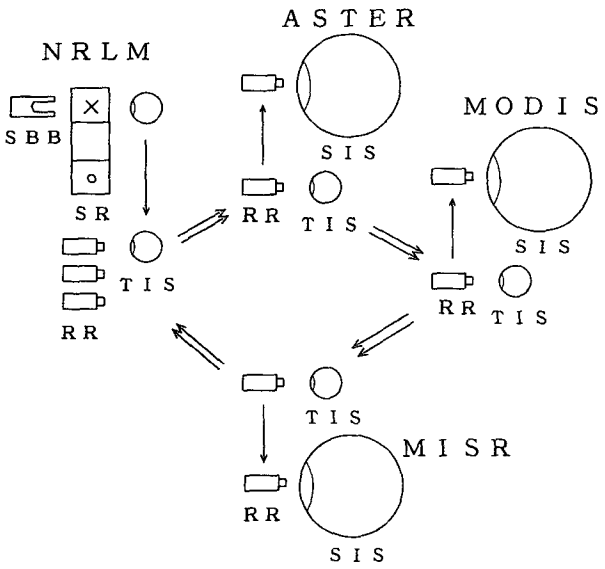

FIG. 5. Round-robin cross-calibration of EOS *AM-1* spherical integrating sources.

At NRLM, three RR radiometers have center wavelengths similar to the ASTER VNIR bands 1–3. The other two have the center wavelengths of SWIR bands 4 and 6. The RR method is shown in Fig. 5. First NRLM characterizes the spectral responsivities of the RR radiometers and the spectral radiances of a transfer integrating sphere (TIS). The RR radiometers then record the radiance from the TIS. The RR radiometers and TIS are transported to the manufacturer of each instrument. The stability of the RR radiometers is checked against the TIS. Finally, the RR radiometers record the radiance from the SIS. Using the relative spectral radiance of the SIS, the spectral radiance of the SIS averaged over each band is calculated. The detectors of the RR radiometers are silicon photodiodes for the VNIR region and germanium and indium–arsenide photodiodes for the SWIR region. The RR radiometers for VNIR have two interference filters, one for defining the band shape and the other for suppressing the out-of-band response.

The RR radiometer developed by The University of Arizona employs a silicon trap detector in the wavelength range from 400 to 900 nm for the comparison between the ASTER, MISR, and MODIS preflight calibration sources in the VNIR. The 10–15-nm-width interference filters of seven MODIS bands are selected by rotating a filter wheel. The procedure used to intercompare the sources is the same as that described above. The RR radiometers for TIR cross calibration purposes are under development.

b. In-orbit cross-calibration

1) CROSS-SENSOR CALIBRATION WITHIN PLATFORM

The ASTER TIR subsystem will not be able to view cold space in its normal operation mode. Good calibra-

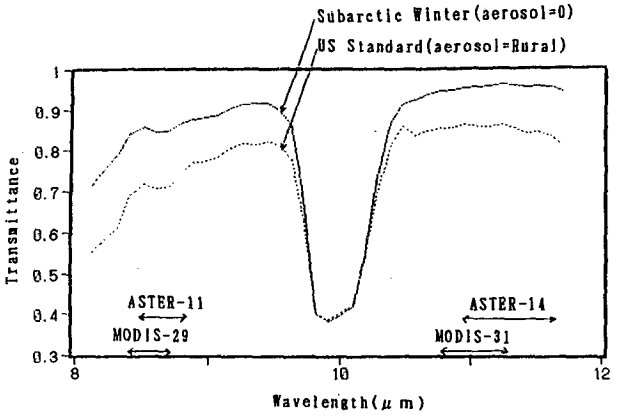

FIG. 6. Atmospheric transmittance for TIR band 11 and MODIS band 29 and for TIR band 14 and MODIS band 31.

tion accuracy is not expected in particular at the low-temperature end of the dynamic range. The ASTER TIR subsystem and MODIS are to be flown on the same platform and will be able to observe, almost simultaneously, the same ground targets through almost the same atmosphere. Thus, by comparing both data, the ASTER TIR will be calibrated with respect to well-calibrated MODIS thermal infrared data. Both sensors, however, have different IFOVs, slightly different bandpasses, and different NEΔTs, and these differences have to be taken into account in the comparison.

To account for the difference of IFOVs between the instruments, an 11 × 11 pixel averaging of the ASTER TIR will correspond approximately to one MODIS pixel at nadir. A comparison of the collocated outputs provides a cross-calibration of the sensors, after the corrections discussed below have been implemented. It is interesting to note that the ASTER TIR when averaged over 11 × 11 pixels yields an NEΔT of 0.03 K if measured in a homogeneous temperature target. This is better than that of MODIS, so that the averaged ASTER TIR data will be useful for the validation of the MODIS NEΔT.

Good collocation accuracy is not expected due to misalignment, thermal stress on the scanning mirror, and so forth. Homogeneous fields, therefore, have to be selected as test sites. To obtain more accurate cross-calibration accuracy at the low-temperature end of the dynamic range, ice and snow in Antarctica and convective clouds are candidate sites. Homogeneity of the scene has to be checked in advance.

TIR band 11 and MODIS band 29 overlap in the wavelength range 8.475–8.7 μm but do not overlap in the wavelength ranges 8.4 and 8.475 μm and 8.7–8.825 μm. Meanwhile TIR band 14 and MODIS band 31 overlap in the wavelength range 10.95–11.26 μm but do not overlap in the wavelength ranges 10.78–10.95 μm and 11.28–11.65 μm. It, therefore, is important to understand the differences in terms of atmospheric transparency and atmospheric radiation in the nonoverlapped wavelength ranges.

TABLE 4. Difference of atmospheric transparency between TIR and MODIS bands.

Sensor	Band	Wavenumber (cm^{-1})	Transparency
TIR	11	1133–1180	0.7518
MODIS	29	1149–1190	0.7337
TIR	14	858–913	0.8484
MODIS	31	887–928	0.8559

Within a scene, homogeneity will be calculated for both the ASTER TIR and MODIS data to be compared by using a homogeneity measure such as the ECHO type of classification method. The error in the radiometric intercomparison of the ASTER TIR and MODIS data due to collocation error will be determined from this homogeneity measure and an estimated uncertainty of half a pixel in the maximum collocation accuracy.

An assessment of cross-calibration accuracy will be conducted with the LOWTRAN-7 code for atmospheric transparency and with the Landsat TM band 6 or *Landsat-3* MSS thermal band data for homogeneous ice and snow scenes or homogeneous convective cloud scenes.

The differences between atmospheric transparency for TIR band 11 and MODIS band 29, and TIR band 14 and MODIS band 31, respectively were assessed with LOWTRAN-7 under the assumption of a 1976 U.S. standard atmosphere and a ground cover of 0% albedo. The transparency of the atmosphere in these wavelength ranges is shown in Fig. 6. These atmospheric transparency characteristics are summarized in Table 4. Table 5 summarizes the accuracy for the proposed cross calibration.

2) CROSS-PLATFORM CALIBRATION AMONG SENSORS

As part of the calibration and validation process, ASTER data will be compared to data collected from sensors on other platforms, such as SPOT and Landsat. These comparisons involve several difficulties that must be overcome to ensure the validity of the cross

TABLE 5. Estimated error of the proposed cross-calibration.

Error source	Percentage	Error at 300 K (K)	Error at 200 K (K)
Atmospheric transparency difference	1.2	0.8	0.3
Collocation error	0.83	0.5	0.2
Spectral emissivity difference	1.0	0.6	0.3
Root sum of squares	1.8	1.1	0.5

calibrations. The most important of these are differences in sun–sensor geometry, ground spatial resolution, and spectral matching (Che et al. 1991). Included in the sun–sensor geometry effects are changes in atmospheric conditions and surface bidirectional reflectance effects.

High-spatial-resolution sensors are the most promising candidates for in-flight cross-calibration. In this case, ground control points can be used to accurately register the different datasets. This will not be possible with low-spatial-resolution sensors and the uncertainties will increase accordingly. Sensors sharing the same platform as ASTER will acquire imagery under identical illumination and viewing conditions, eliminating surface bidirectional reflectance effects and atmospheric changes. Cross-calibration with morning-crossing sensors, such as SPOT and Landsat, will not suffer greatly from these effects, because datasets collected near in time to one other will be used. The spectral mismatch uncertainty will be reduced by carefully selecting ground sites for the cross-calibration studies. The spectral reflectance of these ground sites will be measured and used to correct for spectral mismatch.

In the solar-reflective range, it is estimated that the error due to the misregistration between images will be less than 0.5% and errors due to spectral band mismatch will be less than 1.0%. The atmospheric correction error is expected to be less than 0.5%. Assuming the case for which ASTER is radiometrically corrected to 4%, it should be possible to compare results from other sensors to be better than 4.2% (Che et al. 1991). We do not expect the results to be better than 5% for the case where ASTER is cross-calibrated with an afternoon-crossing sensor having low-spatial resolution.

3) TARGET-RELATED CALIBRATION WITH AIRCRAFT SENSORS

Candidate airborne sensors for cross-calibration with ASTER are the Airborne Visible and Infrared Imaging Spectrometer (AVIRIS), the Airborne ASTER Simulator (AAS), the Thermal Infrared Multispectral Scanner (TIMS), the Thematic Mapper Simulator (TMS), and the MODIS Airborne Simulator (MAS). The characteristics of these sensors are shown in Table 6 (Mah et al. 1993; Ezaka et al. 1993). AVIRIS has about 220 bands to form a 0.4–2.5-μm region that covers the VNIR and SWIR regions. AVIRIS calibration for the VNIR and SWIR of the optical sensors (OPS) on the Japanese Earth Resources Satellite-1 (*JERS-1*) has been carried out since 1992 and some preliminary results have been reported (Green et al. 1993). AVIRIS seems to be a good sensor for cross-calibration with ASTER in the solar-reflection region. AAS has been developed by the Geophysical and Environmental Research Corporation (GER) for the Japan Resources Observation Systems Organization (JAROS). AAS has 1 VNIR band, 3 MWIR bands, and 24 TIR bands from 8 to 12 μm, so it is suitable for ASTER TIR calibration. TIMS with six bands in the TIR region has been developed by JPL and provides coverage for all five ASTER TIR bands. TMS has 12 bands and provides good coverage in the ASTER VNIR region but has only 2 bands in the SWIR region. MAS has 9 bands in the VNIR, 16 bands in the SWIR, 16 bands in the MWIR, and 9 bands in the TIR. This will be useful for cross-calibration between MODIS and ASTER. AVIRIS is preferred to MAS for the cross-calibration of ASTER in the VNIR and SWIR, because of its better spatial and spectral resolution. In all of the above cases the accuracy of the in-flight absolute calibration of the airborne sensor is of paramount importance.

4. Transfer of calibration/characterization from preflight to in orbit using onboard calibrators

In the preflight calibration, the onboard lamps are calibrated against an integrating sphere source by using the radiometer subsystem, and the lamp monitors are calibrated against the imaging radiometer subsystem by using the lamp. The continuity of the preflight calibration data with the in-flight data will be an important concern because the radiometer and the lamps can change during the launch. One of the major causes of change in the radiometer is contamination of the optics by outgassing. A possible cause of change in the lamps is the filament temperature shift due to change in the convection of the gas which fills the lamp bulb (gravity shift). The temperature of the lamp filament may be higher in orbit than on the ground during the preflight calibration, so the effect of the temperature change of the lamp filament on the spectral radiance is measured by the lamp monitors, and a correction table for this change is made.

Figure 7a shows the preflight thermal vacuum calibration data, and Fig. 7b shows the in-flight calibration

TABLE 6. Airborne sensor characteristics.

Sensor	AVIRIS	MAS	TIMS	TMS	AAS
Band number	224	48/50	6	12	28
Spectral coverage (μm)	0.41–2.45	0.53–14.52	8.2–11.8	0.42–14.00	0.7–12
Instantaneous field of view (mrad)	1.00	2.50	2.50	1.25	5.00
Field of view (°)	30	86	77	43	82
Bits per pixel	10	12	8	8	15

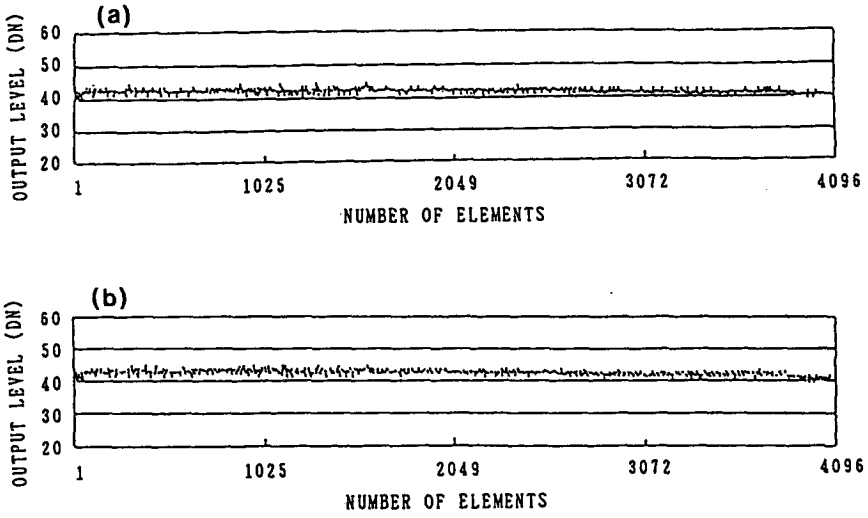

FIG. 7. Preflight thermal vacuum calibration data (a) and in-flight calibration data (b) for 4096 detector elements of the OPS VNIR band 4 against an onboard lamp.

data that were taken 3 weeks after launch for 4096 detector elements of the OPS VNIR band 4 against an onboard lamp. The uniformity of the output DN throughout the CCD was good, and the agreement between preflight and in-flight was within 1 DN, or within 2.5% for all elements. Similar results were obtained for the other OPS VNIR bands. For the OPS SWIR bands, the uniformity of the output DN of the CCD was not as good as for the OPS VNIR, but the agreement between the preflight and in-flight data were at the same level as that for the OPS VNIR bands. The conclusion from these results is that there has been no significant change in the onboard calibration units and the OPS radiometer responsivities during the launch of the *JERS-1,* or the initial in-orbit phase (Hino and Ono 1992).

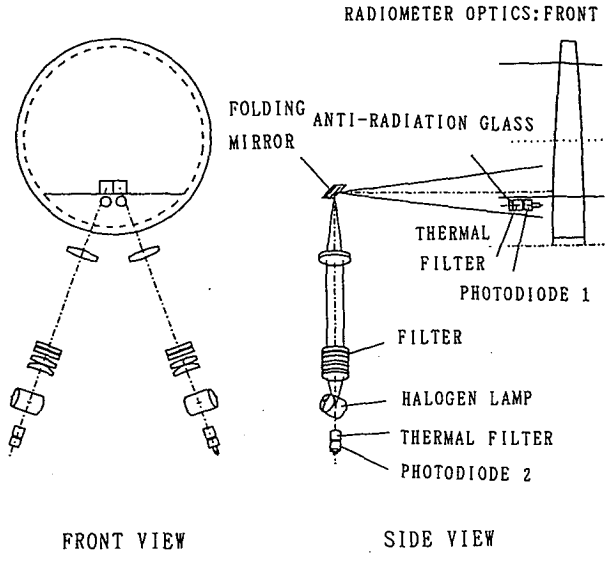

FIG. 8. VNIR onboard calibration units.

5. In-orbit radiometric calibration/characterization methodology

a. Instrument-based calibration

1) REFLECTANCE BANDS

Figures 8 and 9 show layouts of the onboard calibration units for the VNIR and SWIR, respectively. In both cases, the radiation sources are tungsten halogen lamps. A radiant beam from the lamp is fed through calibration optics to the front end of the imaging radiometer subsystem optics. The whole CCD detector is uniformly irradiated by the reference beam. The reference beam is monitored by silicon photodiodes. Each imaging radiometer has two independent, but identical, optical calibration units. The reference beams pass through only a part of the imaging radiometer's aperture, so nonuniform contamination over the aperture may cause a calibration error. The VNIR folding mirror for the reference beam may cause such a nonuniform contamination effect because it modifies the flow of contamination gases in front of the imaging radiometer aperture. To decrease this effect, the folding mirror will be located at a greater distance from the radiometer aperture than was the case with the *JERS-1* OPS.

Simple optics for the onboard calibration unit is desirable to reduce the possibilities of contamination and degradation. The latest plan for the ASTER SWIR onboard calibration units excludes the mirror from the calibration optics so that the reference beam from the halogen lamp reaches the pointing mirror directly without the use of optical components. This option is avail-

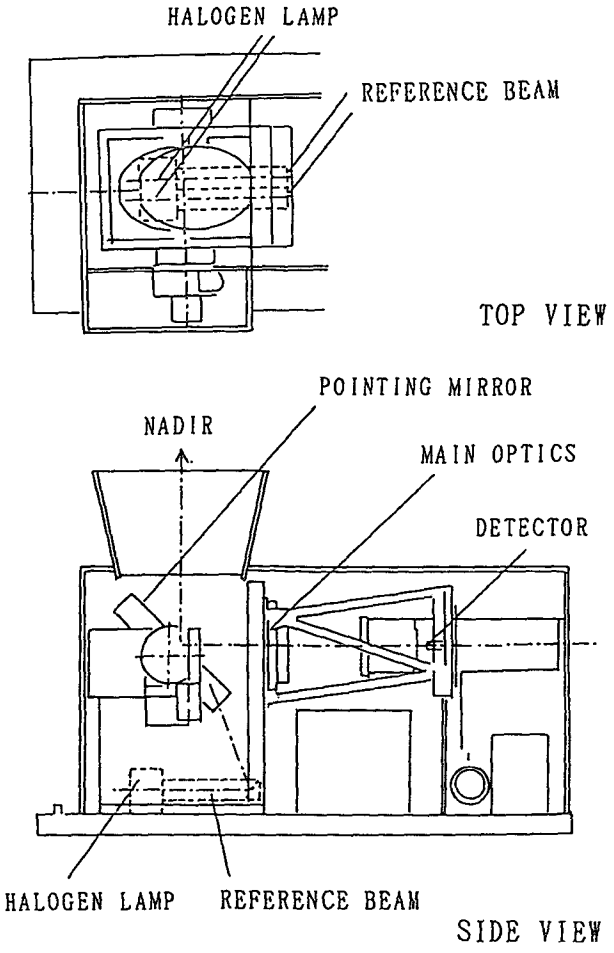

FIG. 9. SWIR onboard calibration units.

able because the lamp radiance is high enough in the SWIR wavelength region. For the VNIR the alternative used is to monitor the halogen lamp radiance directly by a silicon photodiode and to monitor the reference beam just before the VNIR imaging radiometer aperture.

While the nadir-looking telescope of the VNIR has onboard calibration units as described above, the backward-looking telescope has none, because the latter telescope is used only for stereoscopic imaging, and has no calibration requirement. It will be calibrated approximately against the nadir telescope by using uniform test site image data.

Both halogen lamps of the dual onboard calibration units will be operated in orbit once in each recurrent period of 16 days, instead of operating first one lamp and holding the other in reserve. This method of operating both is expected to increase the reliability of calibration because any component which changed can be identified by cross-checking the calibration results.

Table 3 lists an uncertainty estimate of the in-flight calibration. In the in-flight calibration, the gravity shift should be less than ±2%, according to data from the *JERS-1* OPS. In the uncertainty estimate of the onboard calibration, it is assumed that the silicon photodiode is more reliable than the lamp. The lamp and its monitor provide cross-checks and so increase the reliability of calibration. The total uncertainty should be better than ±4%, as required.

2) THERMAL BANDS

There are two modes of in-flight calibration for the TIR, the short-term and the long-term. In the short-term calibration, the temperature of the onboard blackbody will be kept at 270 K and the coefficient D of Eq. (2) will be redetermined if any imaging radiometer change takes place. It is planned to make short-term calibrations just before and just after an observation. In the long-term calibration, the temperature of the onboard blackbody will be changed from 270 to 340 K over a period of 20 min. The coefficients C and D, also A and B if necessary, will be redetermined. The temperature scales from 270 to 200 K and from 340 to 370 K are obtained by extrapolation using Eq. (2). The long-term calibration will be made once in each recurrent period of 16 days.

The TIR radiometer offsets result from background radiation, originally emitted by radiometer components, entering the detector. As the temperature of the TIR radiometer varies, the radiometer offsets drift, so the temperatures of the TIR radiometer components are monitored in orbit and sent to the ground station as telemetry data. The offsets can thus be corrected by using the preflight calibration data.

In order to make an accurate in-flight calibration, the emissivity of the onboard blackbody should be greater than 0.99. The surface structure of the onboard blackbody is under investigation. Methods for blackening the surface are being investigated with respect to the intrinsic emissivity, its reflective specularity, and stability in a vacuum at temperatures from 270 to 340 K. The temperature difference between the thermometer and the radiating surface of the blackbody is expected to be less than 0.2 K. The nonuniformity over the radiating area and stability of the blackbody temperature have yet to be investigated.

Major factors in the uncertainty of the in-flight calibration of the TIR are the emissivity degradation, and temperature uncertainty of the onboard blackbody and its environment. In-flight calibration uncertainty is being analyzed assuming that the emissivity of the onboard blackbody may decrease from 0.995 to 0.985. This will modify the uncertainty in such a way that the onboard blackbody radiance decreases for the high-temperature calibration and increases for the low-temperature calibration, if the reflection components of the environmental radiation are considered. The uncertainties of other effects have been root-sum-squared, then both uncertainties were linearly summed to obtain the

total uncertainties at 270 and 340 K shown in Table 7a. For temperatures below 270 K and above 340 K, estimates of the extrapolation error resulting from the use of Eq. (2) are as listed in Table 7b.

b. *Target-based calibration*

1) GROUND REFLECTANCE AND RADIANCE

The reflectance- and radiance-based methods of vicarious calibration will be used for the in-flight radiometric calibration of ASTER. The reflectance-based approach has a proven history of use since the mid-1980s (Begni et al. 1986; Gellman et al. 1993; Slater et al. 1987; Thome et al. 1993). The radiance-based method has also been used with great success (Biggar et al. 1991; Slater et al. 1987).

The reflectance-based method uses characterizations of a selected test-site surface and overlying atmosphere at the time of satellite overpass. Surface measurements are made for a number of pixels by transporting radiometers across the site and measuring upwelling radiance. Radiance is converted to reflectance through comparisons with measurements of a panel of known reflectance. Atmospheric characterization is performed using solar radiometer measurements that are converted to atmospheric transmittances (Gellman et al. 1991) and used to determine the aerosol properties and columnar absorber amounts over the site (Biggar et al. 1990a; Thome et al. 1992). The results of these measurements are used as input to a Gauss–Seidel iteration radiative transfer code to predict top-of-the-atmosphere radiance (Herman and Browning 1965). The digital numbers reported by the sensor are compared to these predicted radiances to give a radiometric calibration. The atmospheric characterization is improved by measuring the diffuse skylight irradiance and comparing it to the total downwelling irradiance (Biggar et al. 1990b).

The radiance-based method uses an airborne, well-calibrated radiometer to measure radiance instead of surface reflectance. [This is basically the same as the method described in section 3b(3) expect that a simple radiometer is used instead of an imaging sensor.] Since only a minor correction of the measured radiance is needed to account for the intervening atmosphere between the aircraft and the satellite, this method is more accurate than the reflectance-based method.

Both methods rely on selecting the proper site to help reduce the uncertainties in characterizing the radiative transfer of the earth–atmosphere system. In addition to being flat, the surface should have high, uniform reflectance. The overlying atmosphere should have low aerosol loading. A dry climate reduces the chances of cloudiness and the effects of surface moisture. Examples of sites having these characteristics are White Sands Missile Range, New Mexico, and Rogers Dry Lake, California. An alternate site at the Maricopa Agricultural Center, near Phoenix, Arizona, is suitable for verification studies and provides low-reflectance areas.

Biggar et al. (1994) show the reflectance-based calibration method to have an accuracy of 4.9% and the radiance-based method to have an accuracy of 2.8%. When the diffuse skylight measurements are included in the reflectance-based method, the accuracy improves to 3.5%. Improvement to the accuracy of the vicarious calibration are expected from accurate measurements of the surface bidirectional reflectance using a BRDF-camera system currently being developed. Measurements from a newly developed solar aureole camera will improve our knowledge of the aerosol scattering phase function (Grotbeck and Slater, 1993). An automated instrument for measuring the ratio of diffuse to direct irradiance at the ground, and hence deriving the single scattering albedo, is under construction. A spectroradiometer covering wavelengths from 1.1 to 2.4 μm (Smith 1992) will extend the spectral range of our surface reflectance and radiance measurements. A tracking solar radiometer will be improved to collect spectral extinction optical depths from 0.37 to 2.5 μm. With these improvements, it will be possible to calibrate ASTER to better than the required 4% in the solar reflective range.

2) GROUND EMITTANCE

The in-flight calibration of the ASTER TIR subsystem will involve the use of water, land, and cloud-top targets. Water targets will form an important part of the

TABLE 7a. Estimate of the uncertainty of the in-flight calibration of the ASTER TIR at 270 and 340 K.

Calibration temperature (K)	Error factor	Allocated uncertainty (K)
270	Emissivity degradation	0.16
	Onboard blackbody radiance	0.44
	Offset	0.43
	Total	0.78
340	Emissivity degradation	0.33
	Onboard blackbody radiance	0.44
	Offset	0.43
	Total	0.95

TABLE 7b. Total uncertainties of the temperature scale calculated from allocated uncertainties of the in-flight calibration of the TIR.

Temperature (K)	Uncertainty (K)
200	3.00
240	1.23
270	0.78
300	0.71
340	0.95
370	1.10

thermal instrument calibration effort because 1) the emissivity of water is known; 2) the temperature of large areas, compared to an individual ASTER pixel, can be determined with a minimum number of measurements; and 3) the temperature changes slowly enough that defining measurements can be completed before the water temperature has changed by a significant amount.

Land surface will supplement the water targets to estimate the high- and low-temperature calibration of the instrument. Ideal land targets are flat and possess uniform thermal properties. Examples include playas (e.g., Edwards Air Force Base, California), sand sheets (e.g., White Sands, New Mexico), and snow fields. When possible, high-altitude sites will be used to minimize the magnitude of the atmospheric correction and its associated error.

The emissivity of land surface targets will be determined with a field-portable spectrometer and laboratory measurements. Both broadband and ASTER bandpass radiometers will be used to establish the surface radiance and radiance temperature. The sampling strategy will define the surface radiance over areas 3 × 3 pixels (270 m × 270 m) in size or larger. Multiple radiosonde launches will be used to provide control for profiles of atmospheric temperature and water vapor, the principal variables needed to establish an atmospheric correction. Sun photometer measurements will be used to provide aerosol optical depth information and total column water abundance as a check of the radiosonde water vapor profiles.

Land surface targets represent very much more difficult targets to characterize than water targets. This is true with respect to accurate measurement of both spectral emissivity at the scale of an ASTER TIR pixel (90 m) and surface kinetic temperature at the time of *AM-1* platform overflight. Despite these substantial difficulties, such targets represent the only targets available to check the accuracy of the upper end of the ASTER TIR measurement range.

Aircraft thermal scanners (TIMS and AAS) will be used to establish the thermal uniformity of the targets and, if their in-flight calibration can be satisfactorily established, they will be used in a radiance calibration method in which the only correction for the atmosphere is for the atmosphere above the aircraft. Targets will be used extensively at the start of the mission to establish a correspondence between the onboard instrument calibration and the target-related vicarious calibration and continued throughout the mission for calibration control.

3) External lunar reflectance and emittance

Assuming that a spacecraft maneuver to point the nominal nadir direction at the moon is possible, ASTER observations of the sunlight reflected from the moon can be processed to provide a check on the responsivity of the VNIR and SWIR bands, (Kieffer and Wildey 1985). The moon is an object approximately 440 pixels in diameter to the VNIR detectors (220 to the SWIR), and the lunar radiance as a function of phase angle and libration is being determined by a ground-based telescope program, with an absolute radiometric accuracy goal of less than 2% (Kieffer and Wildey 1996) (this telescope program does not extend into the TIR).

A model of this radiance can be interpolated for the precise geometry of an ASTER observation to provide lunar radiance images that can be compared directly with the level 1B product. Although the moon has a reflectance on the order of 10%, the large number of ASTER pixels on the moon can be aggregated to provide an excellent signal-to-noise ratio. The stability of the lunar reflectance (well less than a part per million per year) allows an excellent check of long-term drift of any imaging instrument.

In addition, because the moon represents a circular target against a zero-radiance background, lunar observations can be used to provide an estimate of the MTF and stray-light sensitivity of all bands, including the TIR. The cold space to be viewed during the spacecraft maneuver can provide a zero-radiance background to all bands. It is especially valuable to the TIR because of lack of cold space viewing during the normal observation mode of TIR.

6. In-orbit geometric characterization

Soon after launch, the registration between bands in each telescope will be verified by cross-correlation between images containing many well-defined, high-contrast features. By using some test-site scenes in which many ground control points (GCPs) have been established, the orientation, absolute scale, and pointing relative to the platform reference direction of each array will be verified. The angular resolution of ASTER is smaller than the pointing knowledge of the three subsystems. Thus, cross-correlation between images is required whenever a system pointing is modified. The geometric fidelity of individual bands will depend primarily upon the stability of the spacecraft; however, all ASTER bands except the noncentral SWIR bands are acquired nearly simultaneously, so that correlations between them are not greatly influenced by spacecraft attitude motion.

Because, after initial geometric calibration, there is only one pointing parameter to be determined for each telescope (the cross-track pointing), a single correlation object is adequate in theory.

Strong correlation between the VNIR and SWIR bands is generally expected, and it is anticipated that bands 3 and 4 (near nadir) will provide the best correlation. Small portions of a scene containing sharply defined, high-contrast boundaries (such as road intersections or abrupt topography) will allow correlation to a small fraction of a pixel.

The brightness of the TIR and reflectance bands is expected to be poorly correlated or anticorrelated. However, the positions of boundaries between regions of different materials are expected to be in the same locations in both wavelength regions. For this reason, correlations of boundaries (phase), rather than brightness (amplitude), are preferred.

By using extended boundaries, registration uncertainty can be reduced to a fraction of a pixel; for straight boundaries, this is approximately

$$\frac{(2/N)^{1/2}}{\mathrm{SNR}\, c \sin\theta}, \tag{3}$$

where θ is the angle between the boundary and the alignment direction, N is the number of pixels used, SNR is the signal-to-noise ratio in the brighter region, and c is the fractional contrast across the border.

7. Official calibration algorithm

ASTER, as is the case for many of the EOS sensors, will be calibrated by several different methods to reduce uncertainties and expose and minimize systematic errors. Multiple calibration inputs do, however, introduce the problem of how to combine the results in the most reliable manner to provide the best absolute calibration coefficients as a function of time over the 5-year mission lifetime.

In the case of ASTER, the calibration results will include preflight laboratory calibration of the sensors and the onboard calibrators, preflight cross-calibration of the laboratory calibration sources with other sources from national standards laboratories and other EOS radiometry laboratories, in-flight calibrations using the onboard calibrators, in-flight vicarious calibrations using measured ground (and lunar) reference sites, and in-flight cross-calibrations with other well-calibrated sensors.

Calibration coefficients will be calculated by averaging with weighted functions the calibration data from various calibration methods. It is planned that the calibration coefficients will be reviewed periodically and that the users will be informed of the updated calibration coefficients electronically through an Internet server, for example.

8. Discussion

The discussion of ASTER calibration has been confined here to absolute responsivity. However, the quality of multispectral optical imager data depends on other radiometric and spectral characteristics as well. A calibration requirement document (A. Ono 1994, unpublished manuscript) for the ASTER instrument contractors has been drafted, which deals with spectral and radiometric calibrations comprehensively. This document specifies knowledge requirements of center wavelength and bandwidth of operating bands, offset, nonlinearity of response, absolute responsivity as described here, gain ratio, temperature scale, band-to-band responsivity ratio, element-to-element responsivity ratio in a band, band-to-band temperature-scale difference, element-to-element temperature scale difference in a band, polarization sensitivity, and a control requirement of stray-light rejection.

The specification of stray-light rejection, listed in Table 2, is intended to validate measurement accuracy of earth radiance in orbit. The radiating earth disk subtends a half angle of 64° at the ASTER radiometer entrance aperture at 705-km orbit altitude. The aperture of standard sources does not usually subtend an angle as large as that of the earth's disk. Hence, earth radiance measurements from orbit may be biased by the large subtended angle more than calibration using a standard source. This is the size-of-source effect for radiometer response.

The preflight calibration system developed by NRLM for the reflected solar region is different from other calibration systems using standard lamps of spectral radiance or spectral irradiance. The reason for the adoption of the new calibration system is the anticipated poor accuracy of the SWIR calibration with conventional calibration systems. The conventional spectral radiance standards provided with a strip lamp are based on a blackbody furnace whose temperature is as high as 2000°C. The temperature accuracy of the blackbody furnace depends on the high-temperature standards, which is based on the gold-point temperature defined as 1337.33 K by the International Temperature Scale. The gold-point temperature has been determined by thermodynamically sound measurements such as gas thermometry, total radiation thermometry, monochromatic radiation thermometry, etc. based on the triple point of water defined as 273.16 K.

The spectral radiance levels needed for the SWIR calibration are comparable with blackbody radiation at temperatures from 500 to 700 K as seen in Fig. 1. It is readily understood that a spectral radiance standard lamp is not a good choice as a standard source for the SWIR calibration because it is several steps away from the primary standards; it starts with the triple point of water, step up to the gold point, step up again to 2000°C, and is then stepped down by three or four orders of magnitude to the SWIR calibration level. The present approach is to choose a calibration path as short as possible from the primary standards, recalling that direct access to primary standards provides the highest accuracy.

The most serious limitation to the calibration of sensors on orbit is caused by their inaccessibility to calibration scientists. Stability of onboard calibration units is most critical for successful instrument calibration. However, knowledge of contamination and degradation in orbit is inadequate to meet the instrument calibration requirements completely. Hence it is desirable to make as many checks as possible of the in-flight

calibration. Ground test sites are helpful where optical and radiative properties of test targets are precisely measured and atmospheric absorption and scattering effects are carefully corrected. In-flight cross calibration among the instruments on the same spacecraft where ground common targets are observed simultaneously is also of value.

Acknowledgments. AO, FS, KA, and YY would like to acknowledge the support from the members of the Calibration Working Group in Japan Resources Observation System Organization (JAROS). PNS and KJT wish to acknowledge the support of NASA Earth Observing System Contract NAS5-30781; FDP carried out his research at the Jet Propulsion Laboratory, California Institute of Technology, under contract with the National Aeronautics and Space Administration; HHK is supported by NASA Earth Observing System Contracts S-46459-E and S-19867-E.

REFERENCES

Akasaka, A., M. Ono, Y. Sakurai, and B. Hayashida, 1991: Short wavelength infrared (SWIR) subsystem design status of ASTER. *Proc. SPIE,* **1490,** 269–277.

Aoki, Y., H. Ohmae, and S. Kitamura, 1991: Thermal infrared subsystem design status of ASTER. *Proc. SPIE,* **1490,** 278–284.

Begni, G. M., C. Dinguirard, R. D. Jackson, and P. N. Slater, 1986: Absolute calibration of the SPOT-1 HRV cameras. *Proc. SPIE,* **660,** 66–76.

Biggar, S. F., and P. N. Slater, 1993: Preflight cross-calibration radiometer for EOS AM-1 platform visible and near-IR sources. *Proc. SPIE,* **1939,** 243–249.

——, D. I. Gellman, and P. N. Slater, 1990a: Improved evaluation of optical depth components from Langley plot data. *Remote Sens. Environ.,* **32,** 91–101.

——, R. P. Santer, and P. N. Slater, 1990b: Irradiance-based calibration of imaging sensors. *Proc. IGARSS 90,* Vol. 1, College Park, MD, IEEE Geoscience and Remote Sensing Society and International Union of Radio Science, 507–510.

——, M. C. Dinguirard, D. I. Gellman, P. Henry, R. D. Jackson, M. S. Moran, and P. N. Slater, 1991: Radiometric calibration of SPOT-2 HRV—A comparison of three methods. *Proc. SPIE,* **1493,** 155–162.

——, P. N. Slater, and D. I. Gellman, 1994: Uncertainties in the in-flight calibration of sensors with reference to measured ground sites in the 0.4 to 1.1 μm range. *Remote Sens. Environ.,* in press.

Che, N., B. G. Grant, D. E. Flittner, P. N. Slater, S. F. Biggar, R. D. Jackson, and M. S. Moran, 1991: Results of calibration of the NOAA-11 AVHRR made by reference to calibrated SPOT imagery at White Sands, N.M. *Proc. SPIE,* **1493,** 182–194.

Ezaka, T., Y. Kannari, F. Mills, H. Watanabe, M. Sano, and S. H. Chang, 1993: Laboratory test results for an airborne ASTER simulator. *Proc. SPIE,* **1939,** 210–221.

Fujisada, H., 1994: Overview of ASTER instrument on EOS AM-1 platform. *Proc. SPIE,* **2268,** 14–36.

——, and A. Ono, 1991: Overview of ASTER design concept. *Proc. SPIE,* **1490,** 244–268.

Gellman, D. I., S. F. Biggar, P. N. Slater, and C. J. Bruegge, 1991: Calibrated intercepts for solar radiometers used in remote sensor calibration. *Proc. SPIE,* **1493,** 175–180.

——, ——, M. C. Dinguirard, P. J. Henry, M. S. Moran, K. J. Thome, and P. N. Slater, 1993: Review of SPOT-1 and -2 calibrations at White Sands from launch to the present. *Proc. SPIE,* **1938,** 118–125.

Green, R. O., J. E. Conel, J. van den Bosch, M. Shimada, and M. Nakai, 1993: On-orbit calibration of the Japanese Earth Resources Satellite-1 Optical Sensor using the Airborne Visible-Infrared Imaging Spectrometer. *Proc. IGARSS'93,* Tokyo, Japan, Institute of Electrical and Electronics Engineers and IEEE Geoscience and Remote Sensing Society, 1312–1314.

Grotbeck, C., and R. Santer, 1993: Solar aureole instrumentation and inversion techniques for aerosol studies. Part 2: Data acquisition and inversion. *Proc. SPIE,* **1968,** 566–577.

Hattori, S., and A. Ono, 1982: The effective temperature to express radiant characteristics of nonisothermal cavities. *Temp. Its Meas. Control Sci. Ind.,* **5,** 521–527.

Herman, B. M., and S. R. Browning, 1965: A numerical solution to the equation of radiative transfer. *J. Atmos. Sci.,* **22,** 559–566.

Hino, H., and M. Ono, 1992: Development status of JERS-1 mission equipment—Initial checkout of OPS, MDT and MDR. *J. Remote Sens. Soc. Japan,* **12,** 75–81.

Kieffer, H. H., and R. L. Wildey, 1985: Absolute calibration of Landsat instruments using the moon. *Photogramm. Eng. Remote Sens.,* **51,** 1391–1393.

——, and ——, 1996: Establishing the moon as a spectral radiance standard. *J. Atmos. Oceanic Technol.,* **13,** 360–375.

Mah, G. R., J. C. Eidenshink, K. W. Sheffield, and J. S. Myers, 1993: Earth Observing System precursor data sets. *Proc. SPIE,* **1939,** 250–260.

Ono, A., and F. Sakuma, 1991: ASTER calibration concept. *Proc. SPIE,* **1490,** 285–298.

Sakuma, F., and S. Hattori, 1982: A practical-type fixed point blackbody furnace. *Temp. Its Meas. Control Sci. Ind.,* **5,** 535–539.

——, and A. Ono, 1991: Prelaunch calibration system for Optical Sensors of Japanese Earth Resources Satellite. *Proc. SPIE,* **1493,** 37–47.

——, M. Kobayashi, and A. Ono, 1994: ASTER round-robin radiometers for the preflight cross-calibration of EOS AM-1 instruments. *Proc. IGARSS'94,* Pasadena, CA, Institute of Electrical and Electronics Engineers and IEEE Geoscience and Remote Sensing Society, 1995–1997.

Slater, P. N., S. F. Biggar, R. G. Holm, R. D. Jackson, Y. Mao, M. S. Moran, J. M. Palmer, and B. Yuan, 1987: Reflectance- and radiance-based methods for the in-flight absolute calibration of multispectral sensors. *Remote Sens. Environ.,* **22,** 11–37.

Smith, M. W., 1992: Design and initial performance evaluations of a portable short wave infrared spectrometer. *Proc. SPIE,* **1762,** 118–134.

Suzuki, N., Y. Narimatsu, R. Nagura, F. Sakuma, and A. Ono, 1991: Large integrating sphere of prelaunch calibration system for Japanese Earth Resources Satellite optical sensors. *Proc. SPIE,* **1493,** 48–57.

Takahashi, F., M. Hiramatsu, F. Watanabe, Y. Narimatsu, and R. Nagura, 1991: Visible and near infrared (VNIR) subsystem and common signal processor (CSP) design status of ASTER. *Proc. SPIE,* **1490,** 255–268.

Thome, K. J., B. M. Herman, and J. A. Reagan, 1992: Determination of precipitable water from solar transmission. *J. Appl. Meteor.,* **31,** 157–165.

——, D. I. Gellman, R. J. Parada, S. F. Biggar, P. N. Slater, and M. S. Moran, 1993: In-flight radiometric calibration of Landsat-5 Thematic Mapper from 1984 to present. *Proc. SPIE,* **1938,** 126–160.